# Inter-molecular charge transfer parameters, electron-phonon couplings, and the validity of polaron hopping models in organic semiconducting crystals: rubrene, pentacene and $C_{60}$

Hui Yang[1], Fruzsina Gajdos[1] and Jochen Blumberger[1,2]*

[1]*University College London, Department of Physics and Astronomy, Gower Street, London WC1E 6BT, UK*

[2]*Institute for Advanced Study, Technische Universität München, Lichtenbergstrasse 2 a, D-85748 Garching, Germany*

*email: j.blumberger@ucl.ac.uk

## Abstract

We evaluate the validity of the commonly assumed polaron hopping model for some of the most popular organic semiconductors, rubrene, pentacene and $C_{60}$. This model is based on the assumption that the charge carrier is localized, i.e. forms a polaron that hops from one molecule to the next. We have calculated the relevant inter-molecular charge transfer parameters that determine whether a polaron forms or not: electronic coupling matrix element and reorganization energy for the above materials using quantum chemical calculations and molecular dynamics simulations. We find that neither for rubrene nor pentancene the hopping model is justified due to the relatively large electronic couplings between molecules in the respective herring-bone layers. For $C_{60}$ the coupling matrix elements are smaller and a small but finite barrier for charge transport exists in any transport direction. Despite the theoretical problems surrounding the polaron transport model, we find that mobilities based on this model (as obtained from Kinetic Monte Carlo simulation) reproduce very well the room temperature experimental mobility and anisotropy in pentacene and rubrene. However, it fails to reproduce the correct temperature dependence of mobility, predicting a too shallow decay with temperature compared to experiment. Our results call for further development of more advanced simulation approaches, such as non-adiabatic molecular dynamics simulation and their scale-up to large, application-relevant systems.

## 1. Introduction

Organic semiconductors (OS) are one of the most exciting materials that have been discovered in the last 50 years. Light-weight, flexible and relatively easy to produce from renewable resources, OS combine many desirable properties for thin film electronic devices including organic light-emitting diodes (OLEDs) and organic photovoltaics (OPVs).[1-5] However, one of the drawbacks of OS compared to inorganic semiconductors is their limited conductivity of electrical charges.[1] Improving charge mobility in OS may further advance device efficiency, in particular for OPVs through reduction of electrical resistance and suppression of carrier recombination. Yet, systematic development requires a sophisticated and experimentally-validated model that can guide materials and device design as a true predictive tool.

There are two established models to describe CT in OS, one is based on band theory[6,7] in which the charge carrier electron is assumed to be delocalized like in inorganic semiconductors, and the other is polaron theory[8,9] in which charge carriers are assumed to be localized and hop between molecules. Both models are problematic. Band-theory approaches are inapplicable at ambient temperatures where the mean free path is shorter than the intermolecular lattice spacing.[10] Hence, over the last ten years, most of the theoretical/computational studies have assumed a charge hopping mechanism, but doubt has been cast as well over the validity of this model.[7,11-17] Electronic coupling between sites are typically, though not always, on the same order of magnitude as reorganization energies in these materials (also denoted trapping energy in the materials chemistry literature) making polarons unstable even on the electronic time scale. What further complicates the problem are the large amplitude thermal motions of the organic molecules which are a consequence of the weak dispersion interactions that hold the molecules together. This results in strong thermal fluctuations of site energies (also termed “diagonal electron-phonon coupling”) and electronic coupling (“off-diagonal electron-phonon coupling”).

Recently, advanced simulation methodologies including mixed quantum-classical non-adiabatic molecular dynamics (MQC-NAMD) have been developed in first attempts to address this

challenging problem[16,18-22] (see Ref. [22] for a discussion of some of these works). Here the charge carrier is explicitly propagated in the time-dependent potential created by the nuclei avoiding any *a priori* assumptions of the CT mechanism. For instance, Elstner and co-workers have simulated charge mobilities in 1D chains of organic molecules using Ehrenfest MD with electronic Hamiltonians at the level of self-consistent charge density functional tight binding.[20] Our group has developed a similar approach denoted fragment orbital-based surface hopping which has been successful applied to 1D chains and dimers of simple molecules.[22] Unfortunately, non-adiabatic MD simulations are computationally expensive even when combined with semi-empirical electronic Hamiltonians and applications to extended 3D materials investigated here is still impractical. In addition, MQC-NAMD schemes are not straightforward to apply in practice. Several remedies have been suggested to cure a number of inherent problems such as electronic overcoherence[23-28], trivial surface crossings[19,29,30] and detailed balance[31-33] but their affect on charge mobility calculations in realistic molecular systems has yet to be investigated.

Independent on the actual method used to calculate charge mobility, a careful characterization of the electronic coupling, charge trapping energies and site energies, as well as their thermal fluctuations, is required as a basis for the investigation of the CT mechanism in OS. Here we present calculations of these quantities for three popular and application-relevant OSs: rubrene, pentacene and $C_{60}$ complementing previous studies on the fullerene derivative PCBM[12,14,17] (see Figure 1a-c). The molecules forming these three crystals exhibit an increasing degree of thermal motion. While rubrene molecules are "locked" to their lattice sites due to their bulky substituents, pentacene molecules fluctuate more freely but are still constrained by neighbouring molecules, whereas $C_{60}$ buckyballs show unhindered rotational diffusion above 255 K[34].

We find that in rubrene and pentacene electronic coupling within the conducting herring-bone layers is too large for stable formation of small polarons. In $C_{60}$ electronic couplings are smaller and a finite but very small barrier for electron transfer exists, which however is smaller than the vibrational zero-point energy. The inadequacy of the hopping model becomes apparent for rubrene and pentacene for which a too shallow decay of mobility with increasing temperature is predicted compared with experiment. These conclusions are consistent with previous studies on the fullerene derivative

PCBM[12,14,17] and call for a more advanced treatment of the problem, as for instance offered by explicit charge propagation schemes.

## 2. Simulation details

**Molecular model systems.** Simulations were carried out using a combination of molecular dynamics (MD) simulation and quantum chemical calculations. Three supercells were generated containing 54 pentacene[35], 108 rubrene[36] and 108 $C_{60}$ molecules[37], respectively, by replicating the respective crystal unit cells three times along each crystallographic axes. The neutral charge state of the molecules was modeled with the generalized Amber force field (GAFF)[38]. The positively charged states for pentacene and rubrene and the negatively charged state for $C_{60}$ were parametrized to reproduce the reorganization energy ($\lambda$) for charge transfer between the corresponding dimers at infinite separation at the density functional theory (DFT) level. To this end, the restrained electrostatic potential (RESP) atomic charges of the charged molecules were computed using the B3LYP functional[39]/6-311G* basis set, and used as atomic point charges in the force field description. Then, the position of the minimum of the C=C harmonic bond potential was adjusted so that the reorganization energy at the force field level matched the B3LYP/6-311G* reference value as closely as possible. All other force field parameters for the charged molecule are the same as for the neutral molecule. $\lambda$ was obtained from the standard four-point formula, see Ref. [22] for a more detailed explanation. The bond lengths and atomic point charges used are summarized in Figure S1 and Figure S2 for each molecule and charge state, and the resultant reorganization energies at DFT and force field level are summarized in Table 1. Electronic structure calculations were carried out with the Gaussian programme package[40] and force-field calculations/MD simulations with the Amber programme package [41] or NAMD package [42].

**MD simulations.** MD simulations of the crystals were carried out for the neutral system at five different temperatures (100, 200, 300, 400 or 500 K) and at a pressure of 1 bar applying periodic boundary conditions. After equilibration, a trajectory of length 1 ns was run in the NPT ensemble using a Langevin thermostat. This trajectory was used for the calculation of ET parameters (see below). The structure was stable during the finite temperature MD runs with RMSDs between 0.31 –

0.95 Å with respect to experimental crystal structures. The error with respect to the experimental density (where known) was between 1.4-2.7%.

**ET parameters.** 1000 snapshots were taken in equidistant intervals of 1 ps for calculation of ET parameters (electronic coupling matrix elements $H_{ij}$, site energy difference $\Delta E_{ij}$ and free energy difference $\Delta A_{ij}$) and charge hopping rates $k_{ij}$ between adjacent molecules (typically 300-1300 pairs per snapshot). Electronic-coupling matrix elements ($H_{ij}$) were calculated using the ultrafast Analytical Overlap Method (AOM)[43] recently developed in our group. This method is based on a linear approximation $H_{ij} = CS_{ij}$, where $S_{ij}$ is the overlap of the SOMO orbitals of charged donor and acceptor, and $C$ is obtained by calibration to explicit electronic structure calculations, $C$ = 1.819 eV. AOM gives couplings with small mean errors of about a factor of 1.9 over 4 orders of magnitude relative to DFT calculations, but saves orders of magnitude of computational cost[43], see also Ref. [22] for a recent discussion of the method. The site energy difference $\Delta E_{ij}$ is defined as the total potential energy of the system with molecule $j$ charged and all others neutral minus the total potential energy of the system with molecule $i$ charged and all others neutral, both energies evaluated at the same nuclear geometry. The force field parameters for the neutral and charged molecules are used as explained above. Reorganization energy was assumed to be the same for each pair and equal to the intramolecular (or "inner-sphere") contribution, $\lambda_{ij} = \lambda$. The intermolecular (or "outer-sphere") contribution is usually very small in organic semiconductors and is neglected in this work.[13] Free energy differences $\Delta A_{ij}$ for charge hopping were calculated from the mean energy gaps, $\Delta A_{ij} = <\Delta E_{ij}> - \boldsymbol{\lambda}$, where the brackets <….> denote averaging over the MD trajectory. We found that $\Delta A_{ij}$ is vanishingly small for any hopping direction because the molecules $i$, $j$ of the simulated crystals are chemically identical and interact with similar environments. We set this parameter equal to zero.

Table 1. Summary of reorganization energies from DFT and force field calculations.

| molecule | λ from DFT (B3LYP/6-311G*) (meV) | λ from optimized force field (meV) |
|---|---|---|
| rubrene | 152.7 | 151.0 |
| pentacene | 97.9 | 96.7 |
| $C_{60}$ | 105.4 | 104.5 |

**ET rates**. The ET rates $k_{ij}$ are obtained from the semiclassical expression[44,45]

$$k_{ij} = k_{el,ij} u_n \exp\left( - \frac{\Delta A_{ij}^{\dagger}}{k_b T} \right) \tag{1}$$

where $\kappa_{el,ij} = \kappa_{el,ij}(H_{ij}, \lambda, \upsilon_n)$ is the electronic transmission coefficient (see e.g. Ref. [46]) for an explicit expression), $\Delta A_{ij}^{\dagger}$ is the ET activation free energy which takes the form[22]

$$\Delta A_{ij}^{\dagger} = \frac{\lambda_{ij}}{4} - \left( |H_{ij}| - \frac{1}{\lambda_{ij}} |H_{ij}|^2 \right) \tag{2}$$

for $\Delta A_{ij} = 0$, and $\upsilon_n$ is the effective nuclear frequency along the reaction coordinate. In our previous works a formula slightly different from Eq. 2 was used, which assumed that the minimum of the adiabatic ground state coincides with the minimum of the initial diabatic state [13,14,46-48]. This is an approximation and should be replaced by Eq. 2. We note that the expressions Eqs. (1) and (2) are valid in both the non-adiabatic and adiabatic limits and any intermediate regimes. The first term on the right hand side of Eq. 2 is the usual expression for non-adiabatic (Marcus) ET. The second term is a correction that becomes important in the adiabatic regime, where electronic coupling is typically an order of magnitude smaller than reorganization free energy. The effective frequency was obtained according to Eq (3)

$$u_n = \frac{1}{2\pi\lambda} \frac{2}{\pi} \int_0^{\infty} d\omega \omega \frac{J(\omega)}{\omega} \tag{3}$$

where $J(\omega)$ is the spectral density function, $\frac{J(\omega)}{\omega} = \frac{1}{2k_B T} \int_0^{\infty} dt \left\langle \delta\Delta E(0) \delta\Delta E(t) \right\rangle \cos(\omega t)$. In Eq. (3) each frequency coupling to ET is weighted proportional to its contribution to the reorganization energy, $\lambda = \frac{2}{\pi} \int_0^{\infty} d\omega \frac{J(\omega)}{\omega}$. Therefore Eq. (3) can be considered as a finite temperature, non-harmonic extension of the weighting procedure by Huang and Rhys. Here, the spectral density function $J(\omega)$ is obtained from MD simulation for the neutral crystalline systems at 300 K. Trajectories of length 100 ps are run and the site energy difference for a selected donor acceptor pair, $\Delta E$ used for the calculation of the site energy time correlation function $\left\langle \delta\Delta E(0) \delta\Delta E(t) \right\rangle$. This gives

values $\upsilon_n/c$ = 1539 $cm^{-1}$, 1399 $cm^{-1}$ and 1624 $cm^{-1}$ for pentacene, rubrene, and $C_{60}$, respectively ($c$ the speed of light). The difference in effective frequency for the different donor-acceptor pairs within the same crystal can be neglected.

**Charge mobility.** The microscopic rate constants for charge hopping were used to obtain macroscopic charge mobilities using an in-house developed kinetic Monte Carlo simulation programme that implements the Borz-Kalos-Lebowitz (BKL) algorithm[49]. The diffusion of only a single excess charge in the crystal is considered, hence the simulations correspond to the limit of low charge carrier concentration. For each of the 1000 structures sampled along the 1 ns MD trajectory KMC simulation of charge carrier diffusion is carried out (at fixed nuclear positions). The successive Cartesian coordinates $R_i(t)$, $i = x,y,z$, of the centre of mass of the molecule carrying the excess charge were monitored along a KMC trajectory and the diffusion tensor $D_{ij}$ calculated from the mean square displacements, $2D_{ij}t = \left\langle \left(R_i(t) - R_i(0)\right)\left(R_j(t) - R_j(0)\right) \right\rangle$ where the bracket indicates averaging over about 1000 KMC trajectories per structure. The mobility tensor was obtained using the Einstein relation, $\mu_{ij} = qD_{ij}/(k_BT)$, followed by diagonalisation. The eigenvalues of the mobility tensor thus obtained were averaged over all MD configurations.

## 3. Results and discussion

### Thermal distributions of electronic couplings

The thermal distribution of electronic couplings $H_{ij}$ are shown in Figure 1 (d)-(f) for rubrene, pentacene and $C_{60}$ at room temperature (300 K). They span about 5 orders of magnitude from $10^{-3}$ to ~200 meV. For rubrene and pentacene the total distribution is broken down in distributions for nearest neighbour pairs along the directions indicated in panels (a) and (b). The latter are very well approximated by Gaussian fit functions, $P(|H_{ij}|) = A \exp[-(|H_{ij}| - \langle|H_{ij}|\rangle)^2/(2\sigma^2)]$, with $R^2$ values between 0.937-0.998 (see Table 2). Rubrene exhibits the strongest electronic coupling along the P ("Parallel") direction (83.5 meV) due to almost perfect pi-pi stacking in this direction. The coupling between the T-shaped pairs (T) within the same herringbone layer is significantly smaller but still sizable. In pentacene there are no pairs that form ideal pi-stacking interactions as in rubrene but there

are two T-shaped motifs within the herringbone layer (T1 and T2) that exhibit large electronic couplings (62.7 and 44.1 meV, respectively). In both materials the width of the coupling distribution is of the same order of magnitude as the mean, which is a common characteristic of OSs. The mean coupling values obtained here from our ultrafast AOM method are in good agreement with values reported in previous investigations[13,50-52] (see Table 2).

Table 2: Mean values ($<|H_{ij}|>$) and root-mean square fluctuations ($\sigma$) for electronic coupling matrix elements for inter-molecular hole transfer in rubrene and pentacene and for electron transfer in $C_{60}$.[a]

| crystal | dimer type | distance of center of mass (Å) | $<\|H_{ij}\|>$(meV) | $\sigma$ (meV) | correlation coefficient [b] | $<\|H_{ij}\|>$ literature values (meV) |
|---|---|---|---|---|---|---|
| rubrene | P | 6.8 | 83.5 | 17.3 | 0.980 | 78 [e], 107[f] |
| | T | 8.0 | 19.3 | 11.7 | 0.997 [c] | 10 [e], 21[f] |
| pentacene | T1 | 4.8 | 62.7 | 26.4 | 0.937 | 96.7 [g], 81[f] |
| | T2 | 5.2 | 44.1 | 22.5 | 0.979 | 64.0 [g],68[f] |
| | P | 6.3 | 17.6 | 12.0 | 0.985 | 41.7 [g],39[f] |
| $C_{60}$ | P | 14.2 | 16.7 | 3.9 | 0.998 [d] | 14 [h] |

a. All $H_{ij}$ values reported are obtained from the analytic overlap method (AOM)[43] and averaged over a 1 ns MD trajectory at 300 K.

b. Fit to a single Gaussian $P(|H_{ij}|) = A \exp(-(|H_{ij}| - <|H_{ij}|>)^2/(2\sigma^2))$, unless noted otherwise.

c. Fit to two-Gaussians $P(|H_{ij}|) = A_1 \exp(-(|H_{ij}| - <|H_{ij}|>_1)^2/(2\sigma_1^2)) + A_2 \exp(-(|H_{ij}| - <|H_{ij}|>_2)^2/(2\sigma_2^2))$.

d. Fit to a log-normal distribution ($\log(|H_{ij}|)$ instead of $|H_{ij}|$).

e. Ref. [50]. $H_{ij}$ values were obtained using a fragment orbital approach and Zerner's intermediate neglect of differential overlap.

f. Ref. [51]. $H_{ij}$ values were obtained by the energy-splitting-in-dimer (ESID) method, where the electronic coupling is approximated to be half of the energy splitting between the HOMO and HOMO-1 in the dimer, in case where charge transfer from HOMO of molecule 1 to HOMO of molecule 2 is considered.

g. Ref. [52].

h. Ref. [13]. $H_{ij}$ values obtained from fragment orbital density functional theory (FODFT).

In contrast to rubrene and pentacene, $C_{60}$ (panel f) exhibits only one single peak due to the free rotational diffusion of the buckyballs around their lattice sites at 300 K, averaging out any directional dependence. The distribution is better described by a log-normal distribution ($R^2$= 0.998) than by a Gaussian ($R^2$= 0.979) due to a long tail at larger coupling values. A similar observation has been made for the $C_{60}$ derivative PCBM in Ref.[12]. We also note that the mean coupling value for $C_{60}$ (16.7 meV) is much smaller than for rubrene and pentacene. This is a consequence of the large spatial extent of the SOMO orbital of $C_{60}^-$ and the small orbital coefficients on any of the carbon atoms including the ones on donor and acceptor that are in van-der Waals distance and contribute most to the coupling. Evidently, the isotropy of electronic coupling and charge mobility in room temperature

$C_{60}$ (which is beneficial in actual devices) is paid for by the modest electronic coupling strength.

The sensitivity of the coupling distribution with respect to a change of temperature is shown in Figure 1 (g-i). We find three qualitatively distinct *T*-dependences for rubrene (panel g), pentacene (panel h) and $C_{60}$ (panel i). The distribution for rubrene is found to be very robust in the wide temperature interval 100-500 K. The qualitative features in the distribution are retained even at temperatures as high as 500 K. The peaks just become slightly wider and shift to somewhat smaller values. By contrast, the peaks for pentacene gradually disappear and coalesce to a smooth distribution as the temperature is increased, whereas for $C_{60}$ the peaks gradually merge in a single, broad peak.

The different behaviour is due to the different packing structure and degree of orientational disorder of the molecules. Whilst the rubrene molecules are "locked" to their lattice sites by the bulky phenyl groups, the pentacene molecules undergo strong hindered rotations around their lattice sites as the temperature is increased. Hence, pentacene becomes structurally much more disordered than rubrene as the temperature is increased, resulting in a continuous, featureless coupling distribution at 500 K. The effect of thermal motion is even more pronounced in case of $C_{60}$ (panel i). Below 255 K rotation of the buckyballs around their lattice sites is hindered[34] resulting in a peaked distribution. Above that temperature they have enough kinetic energy to rotate freely. The molecules are then orientationally fully disordered, resulting in a single smooth distribution.

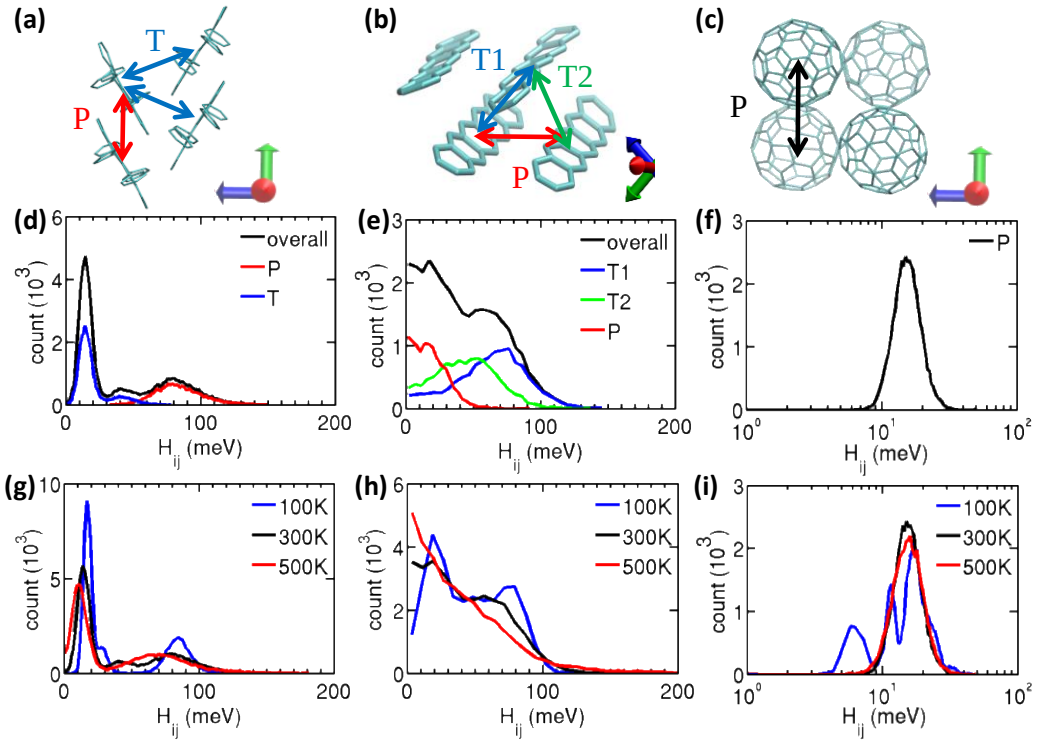


Figure 1. **(a)-(c)** Orientation of nearest neighbour molecular pairs in pentacene (a), ruberene (b) and $C_{60}$ (c) crystals. Arrows at the right bottom corner in each panel point in the direction of eigenvectors of the mobility matrix for each system (for numerical values, see Figure 5 where the same colour code is used.) **(d)-(f)** Distribution of electronic coupling matrix elements $|H_{ij}|$ for hole transfer between nearest neighbor pairs in rubrene (d) and pentacene (e), and for electron transfer in $C_{60}$ (f). The data are obtained from 1 ns MD simulation at 300 K. The overall distribution is shown in black and the decomposition in contributions from different directions is shown in colour. P and T denote parallel and transverse direction, respectively. **(g)-(i)** The overall distributions of electronic coupling matrix element for all nearest neighbor pairs at different temperatures for rubrene (g), pentacene (h) and $C_{60}$ (i).

**Thermal distributions of site energies**

The thermal distributions of site energy differences between molecules, $\Delta E_{ij}$, are shown in Figure 2 (a). They are well described by Gaussian distributions centered at zero mean. The mean gap vanishes because the molecules *i*, *j* are chemically identical and interact with similar environments. The width of the distributions is significantly larger for rubrene than for pentacene or $C_{60}$ in accordance with the larger inner sphere-reorganization energy $\lambda_i$ for rubrene. In addition, we find that the width increases linearly with temperature and the slope is approximately proportional to $\lambda_i$ (Figure 2 (b)). This can be

understood by the well known relation for Gaussian energy gap distributions[46], $\sigma^2 = 2k_B T\lambda$, implying that $\lambda$ is virtually $T$-independent.

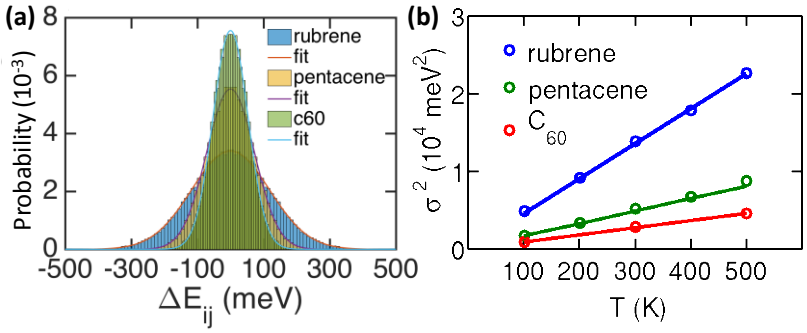


Figure 2. (a) Distribution of site energy difference from 1ns-long MD simulation for nearest neighbours at 300K. (b) Linear relationship between variance of site energy difference and temperature.

**Timescales of fluctuations**

An analysis of the time scale of the fluctuations gives a complementary perspective on electronic couplings and site energy difference. Besides, it gives insight how those energies should be averaged for the calculation of ET rates. To this end we have carried out a frequency analysis of the fluctuations for a single CT event between two nearest neighbour molecules (Figure 3). For rubrene and pentacene the electronic coupling fluctuations extend from the nanosecond domain (lower limit of our simulation) well into the 0.1 ps regime (100 $cm^{-1}$) typical of low frequency molecular motion (e.g. hindered rotations). Therefore, the coupling fluctuations strongly overlap with the spectrum for the site energy difference. The situation is different for $C_{60}$. The coupling fluctuations (1-10 ps) are slower than for rubrene/pentacene due to slow rotations of $C_{60}$ (high moment of inertia) correlating well with the orientational correlation time of $C_{60}$ (10 ps) [34]. There is no overlap with the spectrum for site energy fluctuations which is dominated by two high-frequency modes, the C=C stretch (1650 $cm^{-1}$) and breathing mode (485 $cm^{-1}$). This implies that in $C_{60}$ electronic coupling can be considered as static on the time scale of the site fluctuations, whereas in rubrene and pentacene coupling and site energy fluctuations occur on the same time scale.

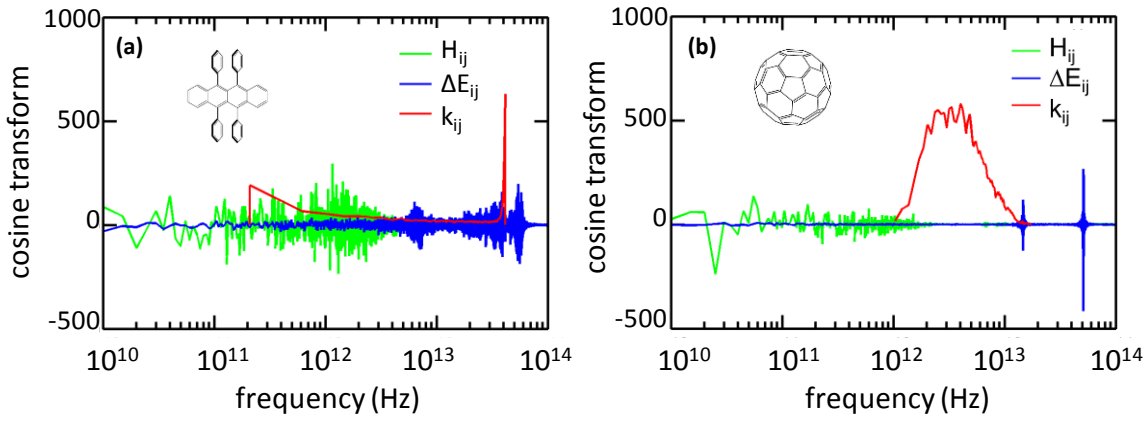


Figure 3. Frequency analysis of ET parameters electronic coupling (green) and site energy difference (blue) for rubrene (a) and $C_{60}$ (b) at room temperature. The distributions for the corresponding inter-molecular charge transfer rates (Eq. 1) are shown in red.

**Existence of small polaron**

Having characterized the magnitude and the thermal fluctuations of electronic couplings and site energy differences, we are now in the position to investigate whether small polarons can form in these materials. This is the case when the nuclear distortions in response to the charging of a molecule *i* create a sufficiently deep potential well so that the excess charge remains localized on the molecule. A necessary condition for small polaron formation to occur is that the activation free energy for charge transfer between the molecules *i* and its neighbours *j*, Eq. 2, is finite, $\Delta A_{ij}^{\dagger} > 0$. Equation 2 implies that the free energy barrier disappears, $\Delta A_{ij}^{\dagger} = 0$ for $|H_{ij}| > \lambda/2$. In this case, charge localized states no longer form and the rate formula Eq. 1 for polaron hopping becomes inapplicable. (For two-state systems Rabi-oscillations occur instead, as discussed previously.[22])

We have calculated the activation free energies Eq. 2 for rubrene, pentacene and $C_{60}$ for the different electronic coupling values obtained from MD by setting $\lambda_{ij} = \lambda_i$ ($\Delta A_{ij} = 0$). This latter choice assumes that the fluctuations of site energy differences determining $\lambda_{ij}$ and $\Delta A_{ij}$ are much faster than for electronic coupling, and can thus be averaged over. According to Figure 4 this is strictly valid only

for $C_{60}$, but one can expect that it gives a reasonable approximation also for pentacene and rubrene, in particular since the effective frequency is similar as for $C_{60}$.

The resultant distributions for activation free energy are shown in Figure 4. We find that for a large fraction of configurations the activation free energies Eq. 2 vanishes (22 % for rubrene and 39 % for pentacene) in which case a small polaron cannot be formed. Unsurprisingly, in rubrene most of the activationless transitions are for the P pairs, and in pentacene for the T1 and T2 pairs, all of which exhibit high electronic couplings. For $C_{60}$ no configuration with vanishing activation free energy was found due to the smaller electronic couplings in this crystal, but a large fraction of activation free energies is below the thermal energy, implying that small polarons would be thermally unstable in this system. These findings are very similar to our results obtained previously for the fullerene derivative PCBM.[14]

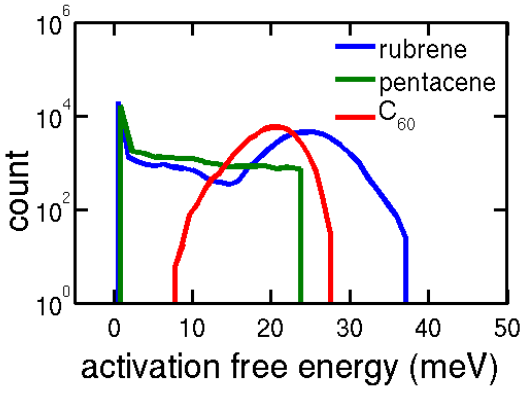


Figure 4. Distribution of activation free energy ( $\Delta A_{ij}^{\dagger}$ , Eq. 2) for inter-molecular charge transfer in rubrene, pentacene and $C_{60}$. Note the peak at vanishing activation free energy ( $\Delta A_{ij}^{\dagger} = 0$) for rubrene and pentacene.

**Charge mobility**

The disappearance of an activation barrier for a significant number of configurations means that the charge carrier will delocalize and possibly form percolation paths. On the other hand, the thermal fluctuations of the site energies and couplings may lead to (temporary) re-localisation of the carrier. Therefore, a good theory for this problem should not make any *a priori* assumptions with regard to the degree of localisation of the charge carrier. In this regard, non-adiabatic molecular dynamics

simulation techniques that explicitly propagate the charge carrier in the time-dependent external (nuclear) potential may present a way forward to deal with this challenging problem. [16,18-22] We have recently developed such a methodology based on Tully's fewest switches surface hopping[22] and successfully applied it to small model systems. Unfortunately, the calculation of charge mobilities for the 3D crystals studied here are still out of reach and will be a major objective of future work. Here we proceed with the calculation of charge mobilities assuming charge hopping even though we know from the above analysis that this model is problematic. Nonetheless, the results obtained for charge hopping are of interest because mobilities obtained from any improved theoretical approach (including non-adibatic MD simulation) will be compared to hopping mobilities as this has been the most popular and widely used model for the last ten years.

Hopping mobilities were calculated for rubrene, pentacene and $C_{60}$ using Kinetic Monte Carlo (KMC) simulation as detailed in section 2. The eigenvalues of the charge mobility tensor obtained for the structures from 1ns MD are shown in Figure 5 (for 300 K), and the averaged eigenvectors are indicated as arrows in Figure 1 (a-c). Rubrene exhibits 2D conduction within the herringbone layer with the highest mobility along the parallel (P) direction ($\mu_1$ = 8.71 $cm^2 V^{-1} s^{-1}$) and a smaller mobility along the direction intersecting the two transverse (T) directions ($\mu_2$ =1.44 $cm^2 V^{-1} s^{-1}$). The mobility along the long molecular axes, perpendicular to the herringbone layers, is nearly zero. Pentacene also exhibits 2D conduction, yet the highest mobility is slightly lower than in rubrene ($\mu_1$ = 4.07 $cm^2 V^{-1} s^{-1}$ along T1) and the anisotropy within the herringbone layer is smaller ($\mu_2$ = 3.19 $cm^2 V^{-1} s^{-1}$ along T2). For $C_{60}$, the room temperature mobility obtained is somewhat smaller than for pentacene ($\mu$ = 3.30 $cm^2 V^{-1} s^{-1}$). Overall, the agreement with previously reported theoretical hopping mobilities is good (see Table 3). Within the hopping model used, mobility can be easily understood in terms of the electronic coupling strength along the respective hopping directions because all other ET parameters are the same for the different directions of a given OS or similar for the different OSs investigated.

Table 3: Comparison of computed mobilities from the literature and from current work with experimental mobilities at room temperature. All values given in $cm^2/(Vs)$.

| | rubrene | | pentacene | | $C_{60}$ |
|---|---|---|---|---|---|
| | $\mu_1$ | $\mu_2$ | $\mu_1$ | $\mu_2$ | $\mu$ |
| computed this work | 8.7 | 1.4 | 4.07 | 3.19 | 3.30 |
| computed literature | 8.1[a], 3.1[b], 43[c] | | 3.5[b], 2.2[f] | | 3.0[i] |
| experimental | 20[d], 10[e] | 7.6[d] | 2.3[g], 11[h] | 0.7[g] | 0.5 ±0.2[j] |

[a] Ref. [50], charge hopping model.
[b] Ref. [51], charge hopping model.
[c] Ref. [53], charge propagation using model Hamiltonian.
[d] Ref.[54] Field-Effect-Transistor (FET) mobility, surface of single crystal.
[e] Ref. [55] Hall mobility, surface of single crystal.
[f] Ref. [52], charge hopping model.
[g] Ref. [56] FET mobility.
[h] Ref. [57] Space-charge-limited current (SCLC) mobility as measured. Corrected to $\mu_1 = 35$ $cm^2/(Vs)$ using effective crystal thickness.
[i] Ref. [13], charge hopping model.
[j] Ref. [58], time-of-flight mobility.

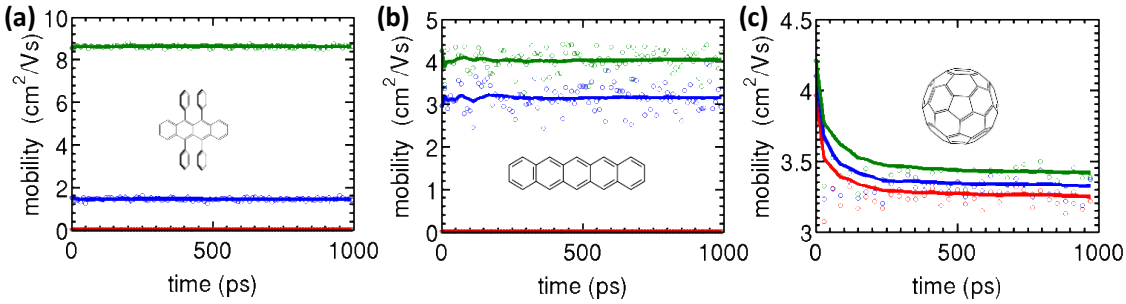


Figure 5. Charge hopping mobilities at room temperature as obtained from KMC simulation. Data points are instantaneous mobility values for snapshots equidistantly spaced along the 1ns trajectory and continuous curves present the accumulated average of the mobilities vs time. The corresponding eigenvectors of the mobility tensor are shown as arrows in Fig 1(a)-(c) using the same color code. The strong thermal fluctuations of pentacene molecules around their lattice sites cause significant fluctuations in instantaneous mobility, in contrast to rubrene where mobility is virtually independent on the structure used. The mobilities for $C_{60}$ become converged only after about 300 ps due to the slow rotational diffusion of the buckyballs.

The room temperature mobilities predicted by the hopping model are in surprisingly good agreement with experimental values[55-61] (see Table 3, deviation of about a factor of 0.09-6.4 depending on the experiment). However, the shortcomings of this model manifest themselves in the temperature-dependence of charge mobility (Figure 6). The mobility decreases with temperature as $T^{-n}$ where n ~ 1 ($n$ = 1.00 for rubrene and $n$ = 1.16 for pentacene), whereas in experiment $n$ = 1.38 for rubrene[55] and $n$ = 2.61 for pentacene[57]. As the hopping rates and diffusion constant obtained from KMC are almost temperature-independent because of the small or vanishing activation free energies for charge hopping, the $T^{-1}$ dependence of charge mobility is simply due to the denominator in the Einstein Equation (Eq. 2). Hence, the hopping model cannot explain the different exponents observed in experiments. This leaves us to conclude that the good agreement with experimental room temperature mobilities is likely to be fortuitous.

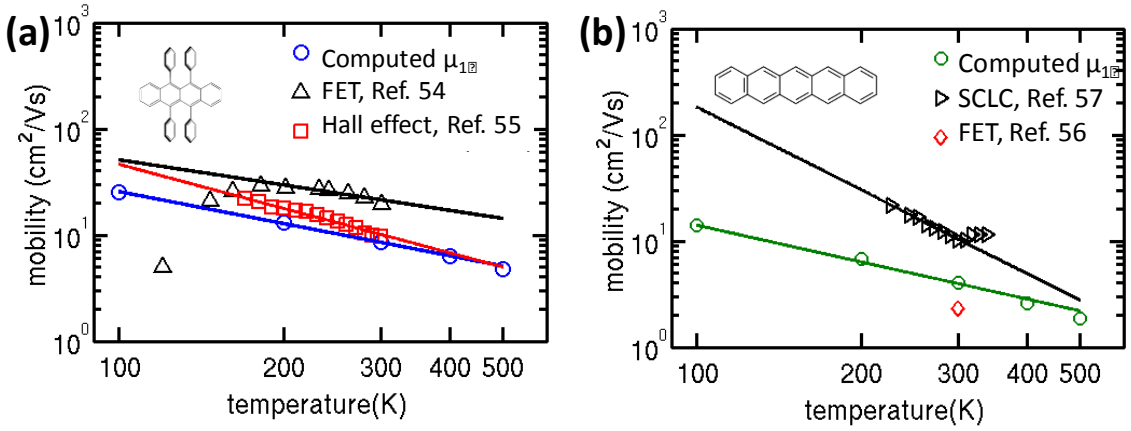


Figure 6. Mobility decay with temperature for rubrene (a) and pentacene (b). Computed hopping mobilities are shown in blue and green symbols and experimental mobilities[54-57] in black and red symbols, respectively. Best linear fits are show in solid lines.

## 4 Conclusion

In this work we have computed the parameters that determine CT in three different OS materials: electronic coupling, reorganization energy and electron-phonon couplings. We find that for a significant fraction of conformations electronic coupling is so large in rubrene and pentacene that a small polaron cannot form. Similar results have been reported for fullerene derivatives by us[14] and

other groups[12,17] suggesting that this is a more general characteristic of (crystalline) organic semiconductors.

Our present work substantiates the view that polaron hopping, the most widely adopted model in the chemistry community for the last ten years, is not sound for the description of CT in crystalline OS.[7] The relatively good agreement between computed hopping mobilities and experimental results near room temperature that is often reported in the literature is likely due to a cancellation of errors. This becomes evident when considering the temperature dependence of mobility in the hopping model. The small activation energies lead to an almost *T*-independent charge diffusion constant at ambient temperatures, resulting in a $T^{-1}$ dependence for any OS investigated. This is in contrast to the experimental *T* dependence, which decays faster and is specific to the OS considered.

We conclude that more advanced simulation approaches are necessary to describe the problem of CT in OS such as non-adiabatic molecular dynamics simulation. First in-roads have been made in this regard[16,20-22], but these methods needs to be made more efficient for application to CT in real 3D systems. In addition, several issues of more fundamental nature need to be addressed and their influence on charge mobility calculations investigated. This includes the type of coupling scheme used for nuclear and electronic motion (Ehrenfest vs surface hopping), the correction schemes used for electronic overdecoherence, the problem of trivial surface crossings as well as the questions of internal consistency of quantum amplitudes and detailed balance. We are currently working on these issues within the framework of our recently developed FOB-SH approach and are confident to apply this methodology in the near future to the systems investigated here. The CT parameters presented in this work provide a sound basis for these future simulations.

**Acknowledgements**

H. Y. acknowledges receipt of a PhD studentship co-sponsored by the Chinese Scholarship Council and UCL. J. B. acknowledges financial support from the European Research Council (ERC) under the European Union's Horizon 2020 research and innovation programme (grant agreement n° 682539/SOFTCHARGE), and the Institute of Advanced Studies at Technical University Munich

(TUM-IAS) for receipt of a Hans-Fischer Fellowship. The authors acknowledge the use of the UCL Legion High Performance Computing Facility and associated support services.

**Supporting information available**

A table summarizing the equilibrium bond lengths and a figure summarizing point charges for rubrene, pentacene and $C_{60}$. This material is available free of charge via the Internet at http://pubs.acs.org.

**References**

(1) Ruiz, C.; García-Frutos, E. M.; Hennrich, G.; Gońez-Lor, B. *J. Phys. Chem. Lett.* **2012**, *3*, 1428.
(2) Kippelen, B.; Bredas, J.-L. *Energy Environ. Sci.* **2009**, *2*, 251.
(3) Fenwick, O. *et al. Nature Nanotechnology* **2009**, *4*, 664.
(4) Brabec, C. J.; Heeney, M.; McCulloch, I.; Nelson, J. *Chem. Soc. Rev.* **2011**, *40*, 1185.
(5) Beiley, Z. M.; McGehee, M. D. *Energy Environ. Sci.* **2012**, *5*, 9173.
(6) Grozema, F. C.; Siebbeles, L. D. A. *Int. Rev. Phys. Chem.* **2008**, *27*, 87.
(7) Troisi, A. *Chem. Soc. Rev.* **2011**, *40*, 2347.
(8) Coropceanu, V.; Cornil, J.; da Silva, D. A.; Olivier, Y.; Silbey, R.; Bredas, J.-L. *Chem. Rev.* **2007**, *107*, 926.
(9) Kim, Y.; Nelson, J.; Zhang, T.; Cook, S.; Durrant, J. R.; Kim, H.; Park, J.; Shin, M.; Nam, S.; Heeney, M.; McCulloch, I.; Ha, C.-S.; Bradley, D. D. C. *ACS Nano* **2009**, *3*, 2557.
(10) Gershenson, M. E.; Podzorov, V.; Morpurgo, A. F. *Rev. Mod. Phys.* **2006**, *78*, 973.
(11) Fratini, S.; Ciuchi, S. *Phys. Rev. Lett.* **2009**, *103*, 266601.
(12) Cheung, D. L.; Troisi, A. *J. Phys. Chem. C* **2010**, *114*, 20479.
(13) Oberhofer, H.; Blumberger, J. *Phys. Chem. Chem. Phys.* **2012**, *14*, 13846.
(14) Gajdos, F.; Oberhofer, H.; Dupuis, M.; Blumberger, J. *J. Phys. Chem. Lett.* **2013**, *4*, 1012.
(15) Gajdos, F.; Oberhofer, H.; Dupuis, M.; Blumberger, J. *J. Phys. Chem. Lett.* **2014**, *5*, 2765.
(16) Ren, J.; Vukmirovic, N.; Wang, L.-W. *Phys. Rev. B* **2013**, *87*, 205117.
(17) Ide, J.; Fazzi, D.; Casalegno, M.; Meille, S. V.; Raos, G. *J. Mater. Chem. C* **2014**, *2*, 7313.
(18) Troisi, A. *J. Chem. Phys.* **2011**, *134*, 034702.
(19) Wang, L.; Beljonne, D. *J. Phys. Chem. Lett.* **2013**, *4*, 1888.
(20) Heck, A.; Kranz, J. J.; Kuba\u{r}, T.; Elstner, M. *J. Chem. Theor. Comput.* **2015**, *11*, 5068.
(21) Pal, S.; J.Trivedi, D.; Akimov, A. V.; Aradi, B.; Frauenheim, T.; Prezhdo, O. V. *J. Chem. Theor. Comput.* **2016**, *12*, 1436.

(22) Spencer, J.; Gajdos, F.; Blumberger, J. *J. Chem. Phys.* **2016**, *145*, 064102.
(23) Prezhdo, O. V.; Rossky, P. J. *J. Chem. Phys.* **1997**, *107*, 5863.
(24) Fang, J. Y.; Hammes-Schiffer, S. *J. Phys. Chem. A* **1999**, *103*, 9399.
(25) Jasper, A. W.; Nangia, S.; Zhu, C.; Truhlar, D. G. *Acc. Chem. Res.* **2006**, *39*, 101.
(26) Granucci, G.; Persico, M. *J. Chem. Phys.* **2007**, *126*, 134114.
(27) Landry, B. R.; Subotnik, J. E. *J. Chem. Phys.* **2012**, *137*, 22A513.
(28) Nelson, T.; Fernandez-Alberti, S.; Roitberg, A. E.; Tretiak, S. *J. Chem. Phys.* **2013**, *138*, 224111.
(29) Nelson, T.; Fernandez-Alberti, S.; Roitberg, A. E.; Tretiak, S. *Chem. Phys. Lett.* **2013**, *590*, 208.
(30) Wang, L.; Prezhdo, O. V. *J. Phys. Chem. Lett.* **2014**, *5*, 713.
(31) Jain, A.; Subotnik, J. E. *J. Chem. Phys.* **2015**, *143*, 134107.
(32) Sifain, A. E.; Wang, L.; Prezhdo, O. V. *J. Chem. Phys.* **2016**, *144*, 211102.
(33) Chen, H.-T.; Reichman, D. R. *J. Chem. Phys.* **2016**, *144*, 094104.
(34) Heiney, P. A. *J. Phys. Chem. Solids* **1992**, *53*, 1333.
(35) Siegrist, T.; Kloc, C.; Schön, J. H.; Batlogg, B.; Haddon, R. C.; Berg, S.; Thomas, G. A. *Angewandte Chemie International Edition* **2001**, *40*, 1732.
(36) Jurchescu, O. D.; Meetsma, A.; Palstra, T. T. *Acta Cryst. B* **2006**, *62*, 330.
(37) David, W. I. F.; Ibberson, R. M.; Matthewman, J. C.; Prassides, K.; Dennis, J. S.; Hare, J. P.; Kroto, H. W.; Taylor, R.; Walton, D. R. M. *Nature* **1991**, *353*, 147.
(38) Wang, J.; Wolf, R. M.; Caldwell, J. W.; Kollman, P. A.; Case, D. A. *J. Comp. Chem.* **2004**, *25*, 1157.
(39) Becke, A. *J. Chem. Phys.* **1993**, *98*, 5648.
(40) Frisch, M. J. *et al.*; Gaussian 03, Revision C.01, Gaussian Inc., Wallingford, CT, 2004.
(41) Case, D. A.; Darden, T. A.; Cheatham, I., T.E.; Simmerling, C. L.; Wang, J.; Duke, R. E.; Luo, R.; Crowley, M.; Walker, R. C.; Zhang, W. *et al.*; AMBER 10, University of California, San Francisco, 2008.
(42) Phillips, J. C.; Braun, R.; Wang, W.; Gumbart, J.; Tajkhorshid, E.; Villa, E.; Chipot, C.; Skeel, R. D.; Kale, L.; Schulten, K. *J. Comput. Chem.* **2005**, *26*, 1781.
(43) Gajdos, F.; Valner, S.; Hoffmann, F.; Spencer, J.; Breuer, M.; Kubas, A.; Dupuis, M.; Blumberger, J. *J. Chem. Theory Comput.* **2014**, *10*, 4653.
(44) Newton, M. D.; Sutin, N. *Annu. Rev. Phys. Chem.* **1984**, *35*, 437.
(45) Nitzan, A. *Chemical Dynamics in Condensed Phases*; Oxford University Press, 2006.
(46) Blumberger, J. *Chem. Rev.* **2015**, *115*, 11191.
(47) McKenna, K.; Blumberger, J. *Phys. Rev. B* **2012**, *86*, 245110.
(48) Blumberger, J.; McKenna, K. *Phys. Chem. Chem. Phys.* **2013**, *15*, 2184.
(49) Bortz, A. B.; Kalos, M. H.; Lebowitz, J. L. *J. Comp. Phys.* **1975**, *17*, 10.
(50) Baumeier, B.; Kirkpatrick, J.; Andrienko, A. *Phys. Chem. Chem. Phys.* **2010**, *12*, 11103.
(51) Kobayashi, H.; Kobayashi, N.; Hosoi, S.; Koshitani, N.; Murakami, D.; Shirasawa, R.; Kudo, Y.; Hobara, D.; Tokita, Y.; Itabashi, M. *J. Chem. Phys.* **2013**, *139*, 014707.
(52) Sokolov, A. N.; Atahan-Evrenk, S.; Mondal, R.; Akkerman, H. B.; Sanchez-Carrera, R. S.; Granados-Focil, S.; Schrier, J.; Mannsfeld, S. C.; Zoombelt, A. P.; Bao, Z.; Aspuru-Guzik, A. *Nat Commun* **2011**, *2*, 437.
(53) Troisi, A. *Adv. Mater.* **2007**, *19*, 2000.

(54) Podzorov, V. M., E.; Borissov, A.; Kiryukhin, V.; Rogers, J. A.; Gershenson, M. E. *Phys. Rev. Lett.* **2004**, *93*, 86602.

(55) Podzorov, V.; Menard, E.; Rogers, J. A.; Gershenson, M. E. *Phys. Rev. Lett.* **2005**, *95*, 226601.

(56) Lee, J.; Roth, S.; Park, Y. *Appl. Phys. Lett* **2006**, *88*, 252106.

(57) Jurchescu, O. D.; Baas, J.; Palstra, T. T. M. *Appl. Phys. Lett.* **2004**, *84*, 3061.

(58) Frankevich, E.; Maruyama, Y.; Ogata, H. *Chem. Phys. Lett.* **1993**, *214*, 39.

(59) Sundar, V. C.; Zaumseil, J.; Podzorov, V.; Menard, E.; Willett, R. L.; Someya, T.; E.Gershenson, M.; Rogers, J. A. *Science* **2004**, *303*, 1644.

(60) Zeis, R.; Besnard, C.; Siegrist, T.; Schlockermann, C.; Chi, X.; Kloc, C. *Chem. Mat.* **2006**, *18*, 244.

(61) Ling, M.-M.; Reese, C.; Briseno, A. L.; Bao, Z. *Synth. Met* **2007**, *157*, 257.